BEFIB2012 – Fibre reinforced concrete
Joaquim Barros et al. (Eds)

NUMERICAL SIMULATION OF THREE-POINT BENDING TESTS: TWO DISTINCT APPROACHES

Vitor M.C.F. Cunha*, Joaquim A.O. Barros†,1 and José M. Sena-Cruz†,2

* ISISE, Dep. Eng., School Science and Tech., University of Trás-os-Montes e Alto Douro
Quinta de Prado 5001-801 Vila Real, Portugal
e-mail: vcunha@utad.pt, vcunha@civil.uminho.pt web page: www.isise.net

† ISISE, Dep. Civil Eng., School Eng., University of Minho
Campus de Azurém 4800-058 Guimarães, Portugal
e-mail:[1] barros@civil.uminho.pt, [2] jsena@civil.uminho.pt, web page: www.isise.net

Keywords: FEM, numerical modelling, indirect tensile tests, fibre reinforced composites.

Summary: *In this work are presented and discussed the numerical simulations carried out for indirect tensile tests of steel fibre reinforced self-compacting concrete specimens. The post-cracking behaviour was modelled with two distinct approaches. Within the scope of the first one, the σ-w relationships were obtained by an inverse analysis procedure up to distinct ultimate crack widths. The other approach consisted on modelling the behaviour of the composite based upon the micro-mechanical behaviour of the fibres. For this purpose the composite was modelled as two-phase material under the FEM basis, with an unreinforced concrete matrix phase (paste + aggregates) and a fibre phase. The fibre phase comprises information about fibre density and orientation depending on where and how the material is applied.*

1 INTRODUCTION

The post-cracking behaviour of a cement based material (either plain or fibre reinforced) can be predicted by the use of a stress-crack opening displacement relationship, σ-w. Regarding plain concrete, the post-cracking behaviour can be characterised by its tensile strength and fracture energy, since the σ-w shape is not too dependent of the concrete strength class, e.g. [1-3]. Furthermore, in general, a bilinear σ-w relationship renders a good estimation of the plain concrete's post-cracking behaviour. On the other hand, for fibre reinforced composites, FRC, the shape of σ-w curves differs considerably depending on the fibre type, content and quality of the concrete matrix. Therefore, for each specific FRC composition it is necessary to determine the σ-w law that best characterizes the mechanical behaviour of the composite in tension. Usually, “indirect” tensile tests are carried out and an inverse analysis procedure is used to determine the best fit parameters of the σ-w curve throughout an optimization procedure [4]. For FRC, and in comparison with plain concrete, it is more suitable to model the post-cracking behaviour with a tri-linear diagram, as used by several researchers, e.g. [5-8], although good results have been achieved with a bilinear diagram [9,10]. The use of poly-linear functions (more than three branches) is another approach for representing the σ-w relationships [11,12], the use of these laws will lead to an increase of the fitting quality. However, some researchers state that this approach will render inconsistent results on the estimation of the first part of the σ-w curve and, particularly, the tensile strength [13,14].

The σ-w relationship may be determined either directly, in a uniaxial tension test (UTT), or indirectly by performing an inverse analysis with test results of three point bending tests (3PBT), split cylinder tests (SCT) or wedge splitting tests (WST). Nevertheless, “indirect” tests methods for determining σ-w

relationship do not gather the consensus of the scientific community, since some held the belief that local minimums of the error function may restrict the inverse analysis from attaining a feasible solution, while others are concerned about the energy dissipated beyond the test end point. Therefore, research based upon indirect test methods should still be validated and calibrated using a "direct" uniaxial tension test. Moreover the post-cracking behaviour of a FRC in a real structure may differ from the behaviour obtained on a test specimen. It is well described in literature that various casting procedures and structural shapes may result in predominant fibre orientation into parallel planes [15,16]. In the case of steel fibre reinforced self-compacting concrete, SFRSCC, the predominant fibre orientation can be along the flow itself (in the fresh state) and along the boundary surfaces due to the wall-effect [17-18]. A predefined orientation of the steel fibres parallel to the tension direction in a test specimen may result in overestimating the post-cracking mechanical properties of the steel fibre reinforced concrete. Therefore, approaching the FRC as a continuum material may lead to a rough estimation, and difficult one, of the mechanical behaviour of a certain FRC structural element. Even though, material behaviour laws for FRC can be obtained with great accuracy by inverse analysis procedures of test specimens, these laws may not translate the accurate material behaviour within a specific structural element.

A fibre reinforced composite can be assumed as a two-phase material, namely, an unreinforced concrete matrix phase and a fibre phase, with the latter one comprising information about fibre density and orientation depending on where and how the material is applied. Hence, this approach can somehow enhance the numerical simulation of FRC structures, thus excluding the use of biased material behaviour laws, i.e. from a macro-mechanical behaviour point of view, obtained from the inverse analysis of experimental tests. In this work are presented and discussed the numerical simulations carried out for indirect tensile tests of steel fibre reinforced self-compacting concrete specimens. The post-cracking behaviour was modelled with two distinct approaches. Within the scope of the first one, the σ-w relationships were obtained by an inverse analysis procedure up to distinct ultimate crack widths. The other approach consisted on modelling the behaviour of the composite based upon the micro-mechanical behaviour of the fibres. For this purpose the composite was modelled as two-phase material under the FEM basis, with an unreinforced concrete matrix phase (paste + aggregates) and a fibre phase. The fibre phase comprises information about fibre density and orientation depending on where and how the material is applied.

2 INDIRECT TENSILE TESTS

2.1 Materials and specimens

The post-cracking behaviour of SFRSCC was assessed with two batches with distinct contents of fibres (Cf), respectively, 30 and 45 kg/m^3. Hooked-end steel fibres with an aspect ratio of 80 and a length of 60 mm were used. Materials and mixture procedure used in the production of the steel fibre reinforced self-compacting concrete, SFRSCC, can be found elsewhere [8]. For each batch eight cylinders with a diameter of 150 mm and 300 mm height were casted, as well as five beams with a cross section of 150×150 mm^2 and a 600 mm length. The compressive strength of each batch was assessed by means of three cylindrical specimens. At the date when the tests were performed (approximately at 30 days), the series with 30 kg/m^3 of fibres, designated by Cf30, had an average compressive strength of 71.1 MPa with a coefficient of variation, CoV, of 1.9%. On the other hand, for the series with 45 kg/m^3 of fibres, Cf45, an average value of 67.2 MPa for the compressive strength, with a CoV of 1.4%, was obtained.

2.2 Tests setup

The tensile behaviour under flexure of the SFRSCC was assessed according to the RILEM TC 162-TDF recommendation [16] (Fig. 1a). Prismatic specimens of 150×150 mm^2 cross section and a length of 600 mm were used. The beams were notched on one of the faces at its mid-span. The width

and depth of the notch was 5 mm and 25 mm, respectively. The specimens were placed on roller supports, giving to the beam a free span of 500 mm.

The specimens used on the splitting tests were obtained from the extremities of the tested bending specimens. For each series, five cubic specimens with a 150 mm edge length were swan out from the prismatic bending specimens. The adopted geometry and dimensions were the suggested by the BS 1981:Part 117 standard [19]. Afterwards, in order to induce the crack plane, two notches were swan upon opposite faces with a 5 mm width and depth of 15 mm. Figure 1b depicts the splitting test's setup. More details about the aforementioned tests set-up could be found elsewhere [8].

(a) (b)

Figure 1: General view of the: (a) Three-point bending test and (b) Splitting test.

3 DETERMINATION OF THE STRESS-CRACK WIDTH LAW BY INVERSE ANALYSIS

3.1 Three-point bending tests

Due to geometry, support and loading conditions, a plane-stress state was assumed. The crack initiation and propagation was modelled with 2D line interface elements located at the specimen's symmetry axis. The remaining part of the specimen was modelled with eight-node Serendipity elements, assuming a linear elastic behaviour. Figure 2 depicts the mesh used in the simulations. For the 2D line interface elements a Gauss-Lobatto integration scheme with three integration points (IP) was used, whereas for the eight-node elements was adopted a Gauss-Legendre integration scheme with 2×2 IP. To avoid undesired spurious oscillations of the stress field a value of 1×10^6 N/mm^3 was used for Mode I initial stiffness modulus [20]. The values of the material properties used in the inverse analysis are comprised in Table 1.

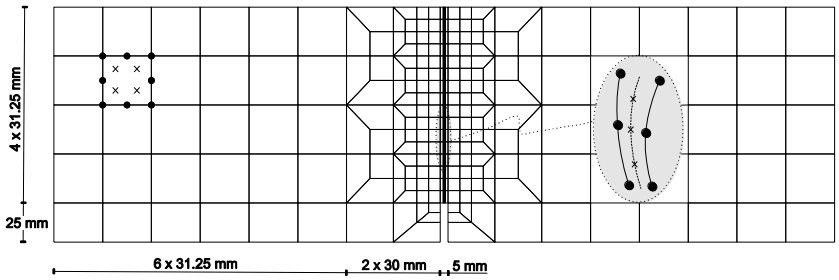

Figure 2: Finite element mesh used in the simulation of the three point bending tests

The inverse analysis (IA) simulations were performed by an exhaustive search method, using for comparison purposes the experimental average curves of each series. The simulations were carried out for two levels of deformation, one using the full load - deflection response (i.e. up to deflection of nearby 9 mm), and another using the response only up to a deflection of 4 mm.

Table 1: Material properties used in the simulation of the three-point bending tests.

Property	Series	
	Cf30	Cf45
Density	$\rho = 2.4 \times 10^{-5}$ N/mm^3	
Poisson's ratio	$\upsilon_c = 0.20$	
Young's modulus	41300 N/mm^2	40600 N/mm^2
Tensile strength	Inverse analysis	
Tri-linear softening parameters	Inverse analysis	

In Figures 3 and 4 are depicted both the experimental and numerical load - deflection curves for the two distinct levels of deformation, respectively, for approximately 9 mm and 4 mm. The agreement between the numerical and the experimental curves is considerably good for both series and both deflection levels, which indicates that the tri-linear σ-w relationship is capable of simulating accurately the post-cracking behaviour of SFRSCC. When comparing the simulations, the numerical curve regarding the Cf30 series response up to a deflection of 9 mm has shown a slightly worse agreement in the pre-peak branch, Figure 3(a). This is ascribed to both the number of branches of the post-cracking law (limited to 3) and to the reason that all stages of the response have the same weight on the fitting procedure. Therefore, in order to attain a good approximation of the full bending response, the initial part of the experimental curve is not so well modelled. On the other hand, the numerical simulation of the Cf30 series response up to a deflection of 4 mm has shown a better agreement with the experimental data for this initial stage of the bending response. This is related with the σ-w law parameters found in the IA that will be discussed in more detail later on.

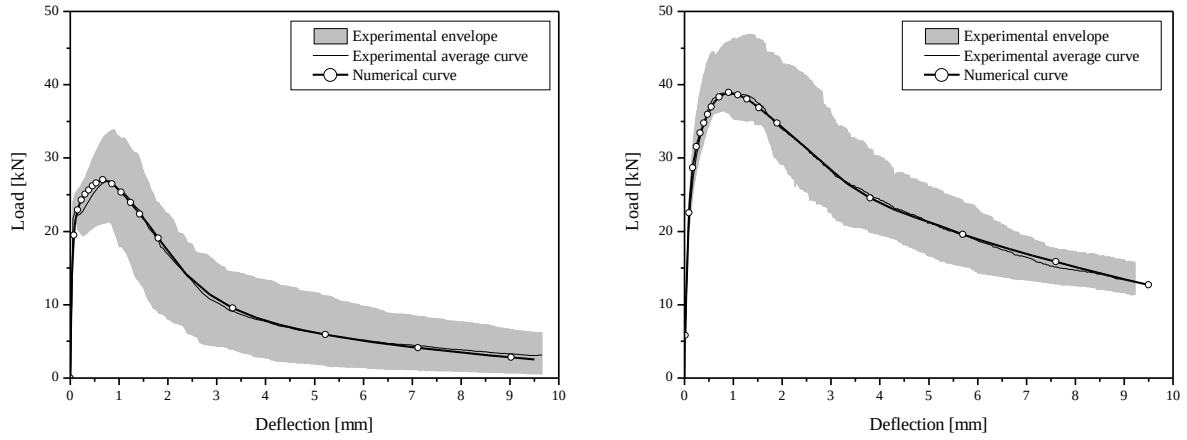

Figure 3: Numerical simulation of the three-point bending tests up to a deflection of 9 mm for: (a) Cf30 and (b) Cf45 series.

The obtained σ-w relationship parameters, and equivalent fitting error (*e*), are indicated in Table 2. At a first glance, it is clear that the σ-w parameters obtained for the Cf30 series are quite different for the distinct deformation levels analysed. In the Cf45 series the values of the parameters are not so distinct for both the studied deflection levels, with the exception of the ultimate crack opening w_u.

Regarding the values found for f_{ct} in the Cf45 series, they are higher than the tensile strength found in the uniaxial tension tests [8] (aprox. 20 to 30%). A similar difference between the tensile strength obtained from indirect and uniaxial tensile tests (11 to 35%) was observed by [12] for conventional fibre reinforced concrete with fibre contents of 39 and 78 kg/m^3. For the Cf30 series, the numerical

simulation up to a deflection of 4 mm provided a value for f_{ct} in good compliance with the uniaxial tensile strength.

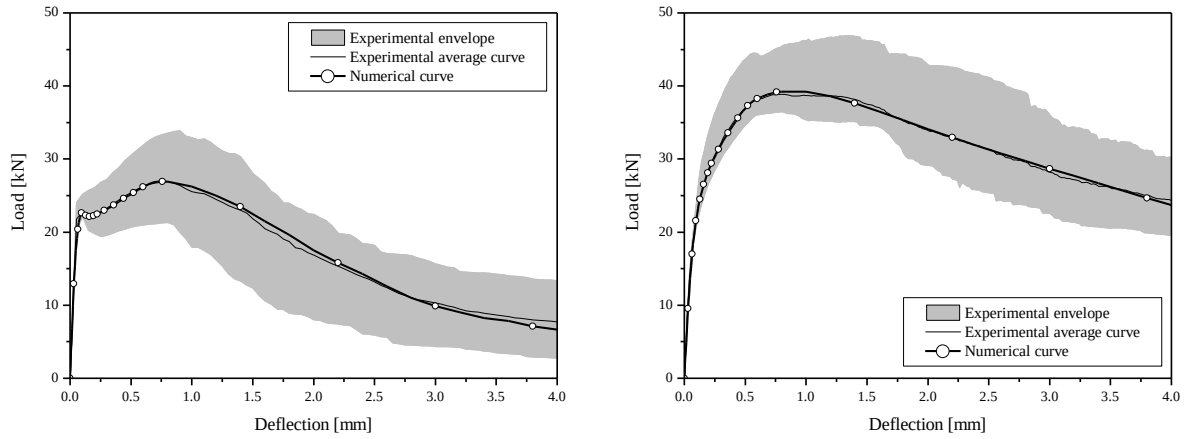

Figure 4: Numerical simulation of the three-point bending tests up to a deflection of 4 mm for: (a) Cf30 and (b) Cf45 series.

The graphical representation of the σ-w law is shonw in Figure 5. Regarding the laws obtained by IA for the Cf30 series, the shape of the initial part of the σ-w law is quite different in case that the IA is performed either up to a 4 mm or 9 mm deflection. In the simulation up to a 4 mm, a sharp load decay is observed on the σ-w law, while for the simulation up to 9 mm, the lower tensile strength obtained in the IA is compensated with a strain hardening in the first post-cracking branch. The higher fracture energy on the σ-w law (until crack widths of 1 mm) for a 9 mm deflection simulation is clearly related in the overestimation on the corresponding experimental load - deflection response; see Figure 3(a). In what concerns to the numerical σ-w relationships obtained for the Cf45 series, up to a crack width of 3 mm the ascertained laws are almost identical, see Figure 5. This is reflected in the numerical load - deflection responses carried out for the Cf45 series, compare Figures 3(b) and 4(b).

Table 2: Parameters of the σ-w relationship obtained by IA

Cf [kg/m^3]		f_{ct} [MPa]	σ_1 [MPa]	σ_2 [MPa]	w_1 [MPa]	w_2 [mm]	w_u [mm]	G_f [N/mm]	e [%]
30	(9 mm)	2.80	2.86	0.56	0.50	2.10	9.0	6.08	2.9
	(4 mm)	3.60	2.45	1.87	0.06	0.89	3.1	4.04	1.8
45	(9 mm)	3.90	4.56	1.99	0.43	2.90	12.0	14.80	1.3
	(4 mm)	3.70	4.66	3.18	0.31	1.72	5.6	11.70	0.9

Note: (f_{ct}, 0), (σ_1, w_1), (σ_2, w_2) and (0, w_u) are the points that define the distinct σ-w relationships

The interest of determining the ultimate crack opening, w_u, for fibre reinforced composites can be questionable, since for practical structural applications the load bearing capacity of these materials will correspond to considerably higher crack opening widths than the usual allowed at the serviceability limit states for the design of a concrete structure. In opposition can be asserted that only with a full knowledge of the material behaviour, hence the knowledge of the ultimate crack width value, there is the possibility of a correct fracture energy estimation and, consequently, the real limit capacity of the structure can be determined.

For determining the ultimate crack width by IA, it is important the level of deformation for which the

numerical analysis is conducted. Even though the present experimental results were obtained for considerable high deformations (over 9 mm), the residual load at these deformations is still considerable, therefore the rest of the bending response, particularly for the Cf45 series, should not be neglected. According to [9], the ultimate crack width can be supposed equal to the average projected embedded length of the fibres, $L_{b,proj}$, defined as:

$$L_{b,proj} = \eta_\theta \frac{L_f}{2} \tag{1}$$

where L_f is the fibre length and η_θ is the fibre effectiveness factor. Remember that the statistical average fibre embedded length, L_b, crossing an active crack is one fourth of the total fibre length [15], thus for the particular used fibres, L_b = 15 mm. If an averaging approach is taken, and assuming for the fibre effectiveness factor a value of η_θ = 0.5 (3D isotropic uniform random distribution), equation (1) will render a value of the ultimate crack opening width, which in practical sense can be regarded as a lower limit for the ultimate crack width ($L_{b,proj}$ = 15 mm).

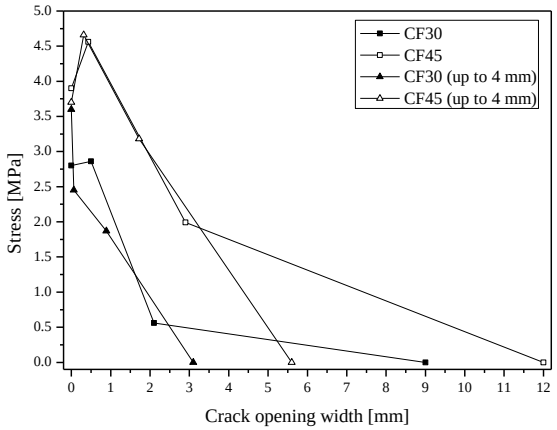

Figure 5: σ-w relationships obtained by inverse analysis.

On the other hand, the fibre effectiveness factor can be computed from equation (2), where N_f is the counted number of fibres at crack section, and A_c, A_f and V_f are, respectively, the beam's net cross section area, the fibre cross section area and the fibre content in volume. In previous work [8], the fibre effectiveness factors was obtained for the Cf30 and Cf45 series, respectively, η_θ = 0.711 and 0.694. These values are within the range of the theoretical values, assuming a uniform isotropic fibre distribution, for the 1D and 2D cases, respectively, 1 and $2/\pi$ [21]. Consequently, by inserting the computed effectiveness factors in equation (1), the ultimate crack width opening will render approximately 21 and 18 mm, respectively, for the series Cf30 and Cf45. These theoretical values are far from the ones obtained from the IA. Hence, this strengthens the idea that the deformation level of 9 mm is not suffice to render an accurate estimation of the fracture parameters, in particular the fracture energy and ultimate crack width.

$$N_f = \eta_\theta \frac{V_f \cdot A_c}{A_f} \tag{2}$$

3.2 Analysis of the parameters obtained from three-point bending and splitting tests

The post-cracking behaviour of the studied steel fibre reinforced self-compacting concrete was assessed from distinct tests, details of the experimental results can be found elsewhere [8]. In Figure 6 are included the stress - crack opening width relationships obtained from uniaxial tensile tests

(UTT), by inverse analysis of the three-point bending tests (3PBT) and from splitting tests (SPLT). The stress - crack opening obtained from the inverse analysis of the three-point bending tests and from the splitting experimental tests clearly overestimates the σ-w relation obtained from the uniaxial experimental tests for both tested series. This was also observed by other researchers for conventional fibre reinforced concrete [10,12,22]. This is due to different fibre structures for each type of specimen, in consequence of distinct concrete casting, different mould dimensions and geometry that induce distinct fibre orientations. It should also be noticed, that the σ-w relationship determined for the splitting tests is not accurate, since it was computed assuming a linear elastic stress distribution.

In order to account the distinct fibre distributions, the σ-w laws obtained from the indirect tests can be corrected using a ratio between the fibre effectiveness factor for the UTT specimens and the fibre effectiveness factor for the indirect tensile tests, ($\eta_{\theta,UTT}/\eta_{\theta,3PBT}$, for the bending and $\eta_{\theta,UTT}/\eta_{\theta,SPLT}$ for splitting specimens). This methodology was used by [22] for correcting the σ-w laws obtained by inverse analysis from 3PBT. Each effectiveness factor is computed from equation (2) using the number of fibres experimentally counted at the crack surface (since for the SPLT tests it was not evaluated the number of fibre at the crack surfaces, it was used the fibre density obtained from an image analysis study [8]). The effectiveness factors obtained are indicated in Table 3. These factors were computed using both the total number of fibres and the effective number of fibres at the crack surfaces. Fibres were considered effective as long their hooked end is deformed or if they have fractured.

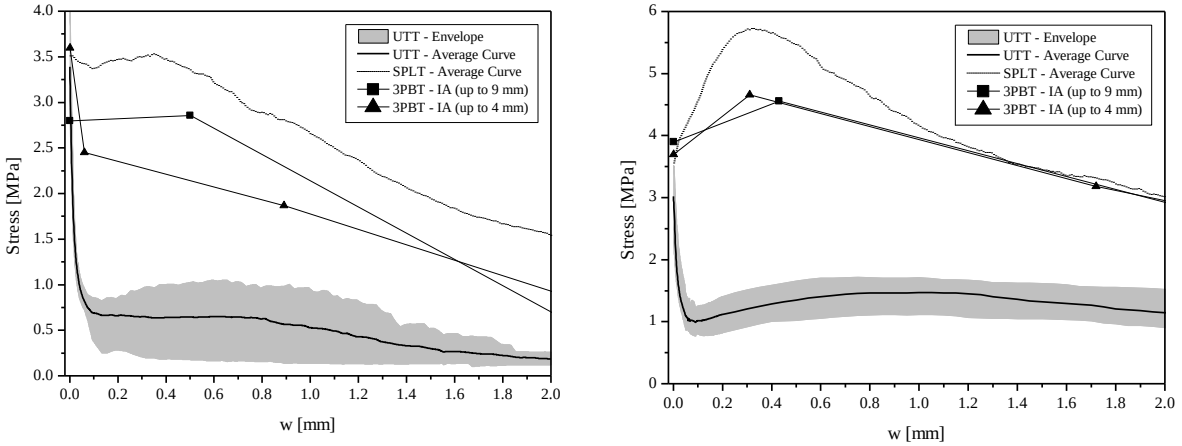

Figure 6: Stress - crack opening laws for the series with: (a) 30 kg/m^3 and (b) 45 kg/m^3.

The σ-w laws corrected with the effectiveness ratio computed from the total number of fibres (e.g. σ $\sigma_i \cdot \eta_{\theta,UTT}/\eta_{\theta,3PBT}$ for the bending tests) can be found in [8]. In general, the Cf30 series had a good agreement with the uniaxial tension behaviour, for both the σ-w relationships from the splitting and bending responses. On the other hand, for the Cf45 series, the uniaxial tension response was still overestimated. The effectiveness factor computed by equation (2) gives an idea of the orientation degree of a certain fibre structure and is related to the number of fibres that intersect a certain plane, since the fibre orientation influences the probability of a fibre crossing a particular surface. Nevertheless, in spite of the effectiveness factor being computed with the total number of fibres, that intersect an active crack, not all the fibres that bridge the crack surfaces may be mobilized and, consequently, contribute for the composite response. A more realistic corrective procedure for the σ-w laws might be assured using the effectiveness ratio computed with the effective number of fibres. In Figure 7 are depicted the σ-w laws obtained by inverse analysis after being corrected according to this

methodology. This approach was not performed for the splitting tests, since there is not available data regarding the number of effective fibres for these specimens.

Table 3: Average fibre effectiveness factors for the distinct tests.

Series	Num. Fibres	$\eta_{\theta,UTT}$	$\eta_{\theta,3PBT}$	$\eta_{\theta,SPLT}$	$\frac{\eta_{\theta,UTT}}{\eta_{\theta,3PBT}}$	$\frac{\eta_{\theta,UTT}}{\eta_{\theta,SPLT}}$
Cf30	Total	0.274	0.711	0.743	0.385	0.369
Cf45		0.454	0.698	0.768	0.650	0.591
Cf30	Effective	0.193	0.656	-	0.294	-
Cf45		0.264	0.576		0.458	

The agreement between the σ-w laws obtained by inverse analysis and the uniaxial tensile response increased significantly for both studied series. However, even using the latter methodology the results for the Cf45 series are still predicting a residual strength higher than the one registered in the UTT. Since the fibre content increased, and, consequently, there are more fibres bridging the crack surfaces, this will favour the concrete's stress redistribution, in spite of the crack progression being forced. Therefore, in the bending tests of the Cf45 series the fracture process zone probably is wider, i.e. diffuse cracking surrounding the main crack. Thus, energy could be dissipated outside the primary crack surface, hence leading to an overestimation of uniaxial tension behaviour by the inverse analysis.

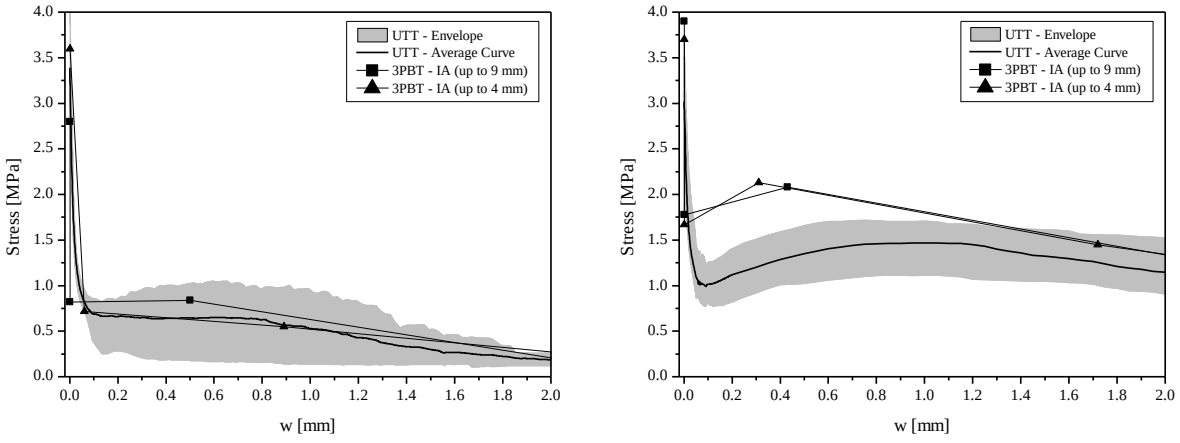

Figure 7: Stress - crack opening laws corrected with distinct effectiveness factors for the series with: (a) 30 kg/m^3 and (b) 45 kg/m^3 (adopting the number of effective fibres).

4 FEM MODEL WITH SHORT DISCRETE FIBRES

The approach comprised within this section consisted on modelling the behaviour of the composite based upon the micro-mechanical behaviour of the fibres. For this purpose the composite was modelled as a two-phase material under the finite element method (FEM), with an unreinforced concrete matrix phase (paste + aggregates) and a fibre phase. The fibre phase comprises information about fibre density and orientation depending on where and how the SFRSCC is applied.

4.1 Random fibre structure generation

In order to model the fibre distribution in a self-compacting concrete medium a numerical code was

developed. This programme, based on the fibre content and geometrical properties of both the fibre and concrete mould, enables to randomly generate a fibre distribution over a specific volume representing a test specimen. In the current algorithm, it is possible to either generate an isotropic uniform random distribution or according to a determinate probabilistic distribution (in order to model the fibre alignment due to the SFRSCC high flowability). In addition, the wall-effect of the mould is also taken into account during the fibre structure generation. For the implementation of the fibre distribution algorithm some considerations and simplifications were made. The fibre thickness was assumed to be null, i.e. the fibre was considered as one-dimensional element and the shape of the end-hooks was also disregarded. Additionally, overlapping between fibres is not checked and therefore allowed. Further details of the developed algorithm can be found elsewhere [8].

4.2 Concrete material modelling

The nonlinear behaviour of the concrete matrix was modelled with a multi-fixed smeared crack model [23]. In the present work, the modelled specimens have a notch to force the occurrence of a single macro-crack in the notched plane; consequently, only one crack is admitted per integration point of the finite element.

4.3 Fibre constitutive law

The present formulation of the embedded fibre model does not take into account fibre bond-slip capability in a direct fashion. Therefore, the embedded cable is modelled with a perfectly bonded assumption. The bond - slip behaviour is simulated in an indirect fashion from the transformation of a load - slip relationship to a tension stress - strain relation. The tri-linear constitutive laws for the embedded cables were determined from fibre pullout tests. Details of the procedure for obtaining the bond – strain relationships for the embedded cables can be found elsewhere [23,24].

4.4 Numerical simulation of the three-point bending tests

The sketch of the finite element mesh used for modelling the concrete matrix phase in the prismatic specimens, for both Cf30 and Cf45 series, is included in Figure 8(a). On another hand, in Figure 8(b) is included a three-dimensional view of the mesh used for modelling the steel fibre phase contribution for the Cf30 series. In the prismatic specimen's finite element mesh are also used Lagrangian 8-node solid elements for modelling the concrete behaviour. The totality of the non-linear behaviour was localized at the notch region, in this specific case at mid-span of the beam. Thus, a $2\times1\times2$ Gauss-Legendre integration scheme is used (1 integration point in the normal direction to the crack surface, i.e. accordingly to the longitudinal axis of the prism. The remaining solid elements are assumed as having a linear elastic behaviour, and a $2\times2\times2$ Gauss-Legendre integration scheme is adopted.

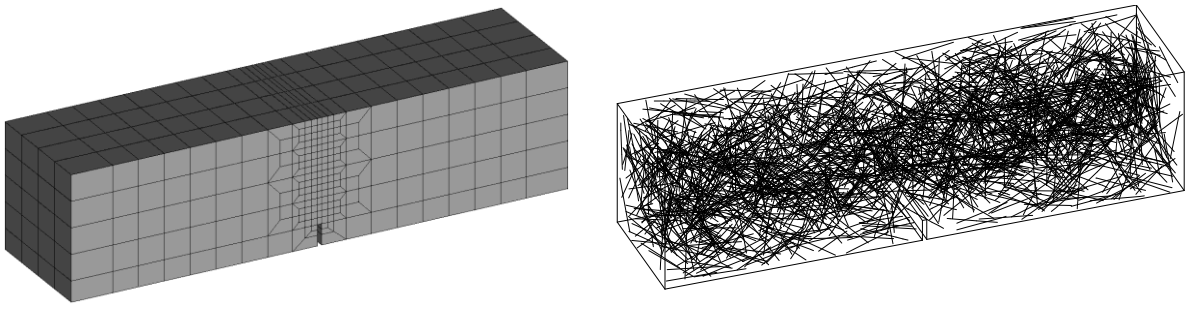

(a) (b)

Figure 8: Three-dimensional finite element mesh of the prismatic specimens: (a) concrete phase and (b) fibres phase (Cf30 series).

The Cornelissen *et al.* [3] softening law was used to simulate the SCC fracture mode I propagation. Table 4 includes the values of the material properties of the concrete used in the current simulations. The steel fibres are modelled with 3D embedded elements with two Gauss-Legendre integration points. For all the embedded elements is assumed a nonlinear behaviour. The parameters for defining the stress - strain diagrams used for modelling the fibres' bond–slip behaviour are comprised in Table 5.

Table 4: Plain concrete properties used in the 3D simulations.

Property	Series	
	Cf30	Cf45
Density	$\rho = 2.4 \times 10^{-5}$ N/mm^3	
Poisson's ratio	$\upsilon_c = 0.20$	
Young's modulous	41300 N/mm^2	40600 N/mm^2
Compressive strength	71.1 N/mm^2	67.2 N/mm^2
Tensile strength	4.6 N/mm^2	4.5 N/mm^2
Fracture energy	0.117 N/mm	0.114 N/mm
Crack band-width	L_b = 5 mm (equal to element height at the notch)	

The numerical simulations of the three-point bending tests are included in Figures 9(a) and (b) for the Cf30 and Cf45 series, respectively. For each series were generated two distinct fibre structures leading to two different numerical responses (Curve A and B, see Figure 9). The agreement between the numerical curve and the experimental results was quite good for both series. Regarding the Cf30 series, the load at crack initiation obtained in the numerical simulation was modelled with accuracy. However, for the numerical curve B a significant load decay is observed down to the lower bound, L.B., of the envelope of the experimental results. Up to a deflection of nearly 0.75 mm, the numerical curve B arises just below the L.B. of the experimental envelope. After the later deflection, the curve is within the experimental envelope.

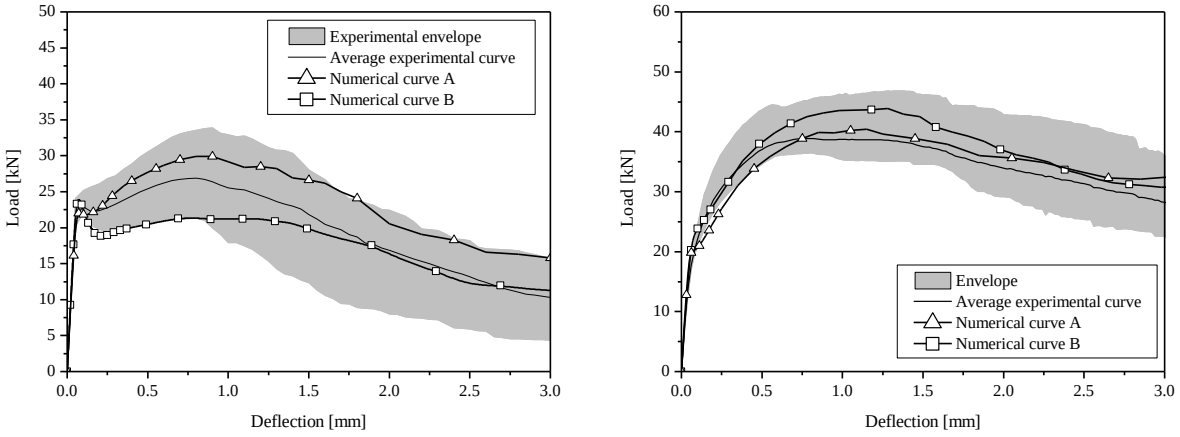

Figure 9: Numerical simulation of the three-point bending tests for: (a) Cf30 and (b) Cf45 series.

On the other hand, the numerical curve A (with a higher number of fibres intersecting the crack plane, see Table 6) was always within the experimental envelope, thus the aforementioned decay was not observed. The agreement between the numerical curves of the Cf45 series and the experimental results was also high. Moreover, the abovementioned load decay was also not observed for neither of the numerical simulations of the Cf45 series.

Table 5: Tri-linear stress–strain diagrams used for modelling the fibres' bond–slip behaviour

α [º]	θ [º]	Series	Failure modes	$\sigma_{f,1}$ [MPa]	$\sigma_{f,2}$ [MPa]	$\sigma_{f,3}$ [MPa]	$\varepsilon_{f,1}$ [-]	$\varepsilon_{f,2}$ [-]	$\varepsilon_{f,3}$ [-]
0	[0, 15[	Cf30 & Cf45	Pullout	588	803	360	0.030	0.090	0.600
30	[15, 45[	Cf30	Rupture	453	679	905	0.016	0.050	0.200
		Cf45	Pullout	588	803	360	0.030	0.090	0.600
60	[45, 75[	Cf30 & Cf45	Rupture	283	362	656	0.020	0.160	0.400

Table 6: Number of fibres and orientation factor at the crack surface of the embedded fibre meshes used for obtaining the distinct numerical curves

	Cf30		Cf45	
Numerical curve	A	B	A	B
Number of fibres	142	105	171	193
Orientation factor	0.780	0.765	0.773	0.761

5 CONCLUSIONS

In this work are presented and discussed the numerical simulations carried out for indirect tensile tests of steel fibre reinforced self-compacting concrete specimens. The post-cracking behaviour was modelled with two distinct approaches. Within the scope of the first one, the σ-w relationships were obtained by an inverse analysis procedure up to distinct ultimate crack widths. The other approach consisted on modelling the behaviour of the composite based upon the micro-mechanical behaviour of the fibres.

The tri-linear post-cracking relationships used in the simulation of the three point bending tests has shown to be capable of modelling the load - deflection curves rather well, even for large deflection levels. The inverse analysis was conducted for distinct deformation levels, up to 4 and 9 mm, and revealed that, even for a large deflection at mid span (9 mm) the ultimate crack opening value estimated is probably incorrect, hence leading to incorrect estimation of the fracture energy. When comparing the σ-w relationships acquired from the indirect tests (3PBT and SPLT) with the uniaxial tension σ-w response a huge discrepancy was observed. This difference was ascribed to the distinct fibre distributions within the specimens used for the different tests. Using a ratio computed based on the fibre effectiveness factor for each type of specimen, a relatively good agreement was observed in both series. Finally, the FEM model with short discrete fibres used for modelling the three-point bending tests rendered a good predictive performance. Thus based on the fibre micro-mechanical behaviour and realistic fibre distribution the behaviour of FRC can be predicted with accuracy avoiding biased laws obtained from inverse analysis.

6 ACKNOWLEDGEMENTS

This work is supported by FEDER funds through the Operational Program for Competitiveness Factors - COMPETE and National Funds through FCT - Portuguese Foundation for Science and Technology under the project SlabSys- HFRC PTDC/ECM/120394/2010.

REFERENCES

[1] P.E. Petersson, "Crack growth and development of fracture zone in plane concrete and similar materials", Report TVBM-1006, Division of building materials, Lund Institute of Technology, Sweden (1981).

[2] P.J. Gustafsson and A. Hillerborg, "Improvements in concrete design achieved through application of fracture mechanics", *in Application of fracture mechanics to cementitious composites. NATO Advanced Research Workshop*, pp. 639-680, USA (1985).

[3] H.A.W. Cornelissen, D.A. Hordijk, and H.W. Reinhardt, "Experimental determination of crack softening characteristics of normal and lightweight concrete. *HERON, Fracture Mechanics and Structural Aspects of Concrete*, 31(2), 45-56 (1986).
[4] P.E. Roelfstra and F.H. Wittmann, "Numerical method to link strain softening with failure of concrete", in *Fracture Toughness and Fracture Energy*, pp. 163-175. Elsevier, London (1986).
[5] A. Hillerborg, "Analysis of fracture by means of the fictitious crack model, particularly for fibre reinforced concrete", *International Journal Composites Cements*, 2(4), 177-184 (1980).
[6] J.A.O. Barros, V.M.C.F. Cunha, A.F. Ribeiro, and J.A.B. Antunes, "Post-cracking behaviour of steel fibre reinforced concrete", *Materials and Structures*, 38(1), 47-56 (2005).
[7] L. Cominoli, A. Medal, and A. Plizarri, "Fracture properties of high-strength hybrid fiber-reinforced concrete", in *Advances in Construction Materials*, pp. 323-332 (2007).
[8] V.M.C.F. Cunha, *Steel fibre reinforced self-compacting concrete - from micromechanics to composite behavior*, Ph.D. thesis, Department of Civil Engineering, University of Minho, Portugal (2010). (http://hdl.handle.net/1822/10667)
[9] A.G. Kooiman, *Modelling Steel Fibre Reinforced Concrete for Structural Design,* Ph.D. thesis, TU Delft, Netherlands (2000).
[10] B.E. Barragán, *Failure and Toughness of Steel Fiber Reinforced Concrete under Tension and Shear*, Ph.D. thesis, Universitat Politecnica de Catalunya, Barcelona, Spain (2002)..
[11] N. Kurihara, M. Kunieda, T. Kamada, Y. Uchida, and K. Rokugo, "Tension softening diagrams and evaluation of properties of steel fiber reinforced concrete. *Engineering Fracture Mechanics*, 65(2-3), 235-245 (2000).
[12] I. Löfgren, H. Stang, and J.F Olesen, "The WST method, a fracture mechanics test method for FRC", *Materials and Structures*, 41, 197-211 (2008).
[13] Y. Uchida and B. Barr, "Tension softening curves of concrete determined from different test specimen geometries", in *Fracture Mechanics of Concrete Structures*, pp. 387-398, Freiburg, Germany (1998).
[14] J. Planas, G.V. Guinea and M. Elices, "Size effect and inverse analysis in concrete fracture", *International Journal of Fracture*, 95(5), 367-378 (1999).
[15] P. Stroeven, "Stereology of concrete reinforced with short steel fibres", *Fract. Mech.Struct. Aspects Concr.,* 31, 15-28 (1986).
[16] RILEM TC 162-TDF, "Test and design methods for steel fibre reinforced concrete - bending test (final recommendation)", *Journal of Materials and Structures*, 35(253), 579-582 (2002).
[17] P. Stähli, R. Custer and J. van Mier, "On flow properties, fibre distribution, fibre orientation and flexural behaviour of FRC, *Materials and Structures*, 41(1), 189-196 (2008).
[18] L. Vandewalle, G. Heirman, and F. Van Rickstal, "Fibre orientation in self-comapcting fibre reinforced concret", in *7th Intnl. RILEM Symposium on Fibre Reinforced Concrete: Design and Applications*, pp. 719-728, Chennai, India (2008).
[19] BS 1981:Part 117, "Testing concrete method for determination of tensile splitting strength", British Standard Institute (1983).
[20] J.C.J. Schellekens, "Interface elements in finite element analysis", Technical report, TU- Delft report 25.2-90-5-17/ TNO-IBBC report BI-90-165 (1990).
[21] P. Stroeven and J. Hu, "Effectiveness near boundaries of fibre reinforcement in concrete", *Materials and Structure*s, 39, 1001-1013 (2006).
[22] M. Strack, "Modelling of crack opening in steel fibre reinforced under tension and bending", in *7th International RILEM Symposium on Fibre Reinforced Concrete: Design and Applications*, pp. 323-332. Chennai, India (2008).
[23] V.M.C.F. Cunha, J.A.O. Barros, J.M. Sena-Cruz, "A finite element model with discrete embedded elements for fibre reinforced composites", *Computers and Structures*, 94–95, 22–33 (2012).
[24] V.M.C.F. Cunha, J.A.O. Barros, J.M. Sena-Cruz, "An integrated approach for modelling the tensile behaviour of steel fibre reinforced self-compacting concrete", *Cement and Concrete Research*, 41, 64–76 (2011).